Stability analysis of H-mode pedestal and edge localized modes in a Joint European Torus power scan

Thawatchai Onjun, Arnold H. Kritz, Glenn Bateman, Vassili Parail, Howard Wilson et al.

Citation: Phys. Plasmas **11**, 1469 (2004); doi: 10.1063/1.1668646
View online: http://dx.doi.org/10.1063/1.1668646
View Table of Contents: http://pop.aip.org/resource/1/PHPAEN/v11/i4
Published by the American Institute of Physics.

Stability analysis of H-mode pedestal and edge localized modes in a Joint European Torus power scan

Thawatchai Onjun, Arnold H. Kritz, and Glenn Bateman
Lehigh University Physics Department, 16 Memorial Drive East, Bethlehem, Pennsylvania 18015

Vassili Parail and Howard Wilson
Euratom/UKAEA, Fusion Association, Culham Science Centre, Abingdon OX14 3DB, United Kingdom

Johnny Lönnroth
Association EURATOM-Tekes, Helsinki University of Technology, P.O. Box 2200, 02015 HUT, Finland

Guido Huysmans
Association Euratom-CEA, CEA Cadarache, DRFC, Batiment 513, 13108 Saint-Paul-Lez-Durance, France

Alex Dnestrovskij
Russian Science Centre Kurchatov Institute, Moscow, Russia

(Received 18 November 2003; accepted 16 January 2004; published online 31 March 2004)

Simulations of three Joint European Torus [P. H. Rebut *et al.*, Nucl. Fusion **25**, 1011 (1985)] type I ELMy high-confinement discharges in a power scan are carried out using the JETTO integrated modeling code [M. Erba *et al.*, Plasma Phys. Controlled Fusion **39**, 261 (1997)] with predictive core and pedestal models, which include the effect of edge localized modes (ELMs). It is found that current-driven peeling modes trigger the ELM crashes in these discharges and, as a result, yield an explanation of the experimentally observed increase in pedestal height with heating power. After each ELM crash, the pressure gradient and the related bootstrap current density at the edge of plasma rapidly increase with increasing heating power, while the total current density rises only slowly because the total current density is impeded by a back electromotive force. Hence, as the heating power is increased, the pedestal pressure can rise to higher values during an ELM cycle before the current density reaches the level required for destabilization of the current-driven peeling modes. In addition, a stability analysis using the HELENA and MISHKA codes [A. B. Mikhailovskii *et al.*, Plasma Phys. Rep. **23**, 713 (1997)] is carried out in conjunction with these simulations. The analysis includes infinite-*n* ideal ballooning, finite-*n* ballooning, and low-*n* kink/peeling modes. © *2004 American Institute of Physics.* [DOI: 10.1063/1.1668646]

I. INTRODUCTION

Energy confinement in the high-confinement (H-mode) regime of tokamaks is found to be quite sensitive to the nature of the pedestal that forms at the edge of H-mode plasmas. The pedestal is a narrow region located near the separatrix, typically occupying less than 5% of the plasma minor radius. It was found in a Joint European Torus (JET) (Ref. 1) power scan that the pedestal height increases with increasing heating power.[2] It is important to understand the physical processes that produce this dependence of pedestal height on heating power in order to develop an improved pedestal model. An improved model is needed for the prediction of plasma profiles in future experiments and of the performance of burning plasma experiments such as the International Thermonuclear Experimental Reactor (ITER).[3]

It was shown in previous studies[4,5] that the pedestal height is independent of heating power when based on the pedestal model in which the pressure gradient near the edge of plasma is limited by the critical pressure gradient of the ballooning mode, without the effect of time-dependent edge localized modes (ELMs). On the other hand, a pedestal model based on concept of thermal conduction[5] yields a pedestal height that increases with heating power. A comparison between the pedestal model using the magnetohydrodynamic (MHD) ballooning approach and a pedestal model based on the thermal conduction approach was carried out in Ref. 5. When compared with experimental data, the thermal conduction pedestal model [Eq. (2) in Ref. 5] yielded a RMSE of 23.5% while the ballooning mode pedestal model [Eq. (5) in Ref. 5] yielded a RMSE of 25.0%. Consequently, in that study, the level of agreement of both pedestal models with experimental data was comparable.

In this paper, the role of heating power in the prediction of the pedestal height is investigated by examining three JET discharges in a power scan. The discharges are type I ELMy H-mode with similar plasma parameters, except for the heating power. It was found that the measured pedestal stored energy and the measured temperatures at the top of the pedestal in these JET discharges increase as the heating power increases.[2] An integrated predictive modeling code, JETTO,[6] is used to carry out simulations of the core and edge plasma for these three JET discharges in order to understand the physical processes that produce this experimental trend. MHD equilibrium and stability analyses codes, HELENA and MISHKA,[7] are used to evaluate the edge stability in these simulations. The instabilities considered include the

infinite-n ideal ballooning, finite-n ballooning, and low-n kink/peeling modes. The results from these simulations and their stability analyses yield a better understanding of the role of heating power in the pedestal physics.

This paper is organized as follows. The transport code, JETTO, and equilibrium and stability codes, HELENA and MISHKA, are described in Sec. II. In Sec. III, the details of the three discharges considered in this paper are described with some discussions regarding an experimental observation. Simulation results and a stability analysis of these simulations are presented in Sec. IV, followed by conclusions in Sec. V.

II. MODELING CODES

In this paper, simulations of a JET power scan are carried out using the predictive JETTO code, while the MHD stability analysis involves use of the HELENA and MISHKA codes. These codes are described in this section.

A. The JETTO code

The $1\frac{1}{2}$D JETTO transport code is used to evolve the plasma current, temperatures and density profiles in both the core and pedestal regions. The core transport is calculated using the mixed Bohm/gyro-Bohm model.[6] For the pedestal region, two assumptions are used in this paper. One assumption is that the turbulent transport is suppressed in the region between the top of the pedestal and the separatrix. For simplicity, all the diagonal elements of the transport matrix within the pedestal are taken to be the ion neoclassical thermal conductivity, calculated at the top of the pedestal using NCLASS.[8] The pedestal width is usually of the order of the ion orbit width (or banana width), which implies limited variation of the neoclassical transport across the barrier. The second assumption regarding the pedestal is that of the pedestal width is either a fixed width of 3 cm, or a width being proportional to the ion Larmor radius. It will be shown later that the variation of the pedestal width by itself is not sufficient to explain the experimental trend observed in this JET power scan.

An anomalous transport is assumed to be present in the core but suppressed within the pedestal region. The reduced transport within the pedestal results in the development of a steep pressure gradient within the pedestal region. This sharp pressure gradient causes an increase in the bootstrap current within the edge transport barrier. The increase of the edge pressure gradient and the resulting increase in edge current density eventually lead to a destabilization of MHD modes. This destabilization then triggers an ELM crash, which results in a loss of plasma energy and particles to the wall. The destabilization is considered to be due to either a pressure-driven ballooning mode[9,10] or a current-driven peeling mode.[11–15]

In exercising the JETTO code, one of two options is employed. In one option, the pressure gradient is allowed to increase until the pressure gradient anywhere within the edge transport barrier exceeds the critical pressure gradient of the ballooning mode. The second option is to allow the pedestal pressure and current to increase until the current-driven peeling mode becomes unstable. With either option, when the instability criterion is met, an ELM crash occurs. Note that the criterion used for the current-driven peeling mode instability is that the edge current density exceeds the critical value predicted using an analytical expression developed in Ref. 13. When the condition for an ELM crash is satisfied, all diagonal transport coefficients in the JETTO code are temporarily increased by 300 times ion neoclassical at the top of the pedestal for electron and ion thermal transport, and 100 times ion neoclassical at the top of the pedestal for particle transport within the pedestal for the specified time interval $\tau_{\mathrm{ELM}}=0.4$ ms, which is of the order of a typical ELM crash duration in JET type I ELMy H-mode discharges. The large increase of the transport within the pedestal leads to a loss of particles and energy, similar to the loss during an ELM crash in the experiment.

TABLE I. Plasma parameters for the discharges used in the power scan obtained from the ITPA Pedestal Database. The plasma parameters (and associated units) are described in Table II.

Plasma parameters	44018	44029	44013
R (m)	2.90	2.90	2.91
a (m)	0.94	0.94	0.94
B_T (T)	2.77	2.77	2.76
I_p (MA)	2.57	2.57	2.57
κ	1.75	1.75	1.75
δ	0.22	0.23	0.23
A_H (amu)	1.97	2.00	1.99
Z_{eff}	1.91	2.05	2.14
n_l (10^{19} particles/m^3)	5.60	5.82	5.82
P_{NBI} (MW)	8.1	11.3	13.9
$T_{e,\mathrm{ped}}$ (keV)	0.72	0.85	0.97
$n_{e,\mathrm{ped}}$ (10^{19} particles/m^3)	4.75	4.76	4.61
$p_{e,\mathrm{ped}}$ (kPa)	5.47	6.43	7.16

B. MHD stability codes

To justify the models used to trigger an ELM crash in the JETTO code, an MHD stability analysis has been carried out using the HELENA and MISHKA codes.[7] HELENA is used to refine the equilibrium and to compute the stability of infinite-n ideal ballooning modes. The HELENA code takes plasma profiles and equilibrium information, generated by JETTO, to produce an equilibrium with the higher resolution that is needed for the MISHKA code. MISHKA is then used to evaluate the stability criteria for finite-n ballooning and low-n kink/peeling modes. In this study, the stability analysis carried out with the MISHKA code is for modes with toroidal mode number $n=1$ to $n=14$. Note that the version of the MISHKA code used in this paper is based on the ideal MHD model.

III. EXPERIMENTAL BACKGROUND

Three JET type I ELMy H-mode discharges in a power scan,[2] JET discharge 44018, 44029, and 44013, are considered in this study. These discharges have the same plasma current, magnetic field, elongation and triangularity, but different heating power. Some of the plasma parameters for these discharges are given in Table I. Figure 1 shows the

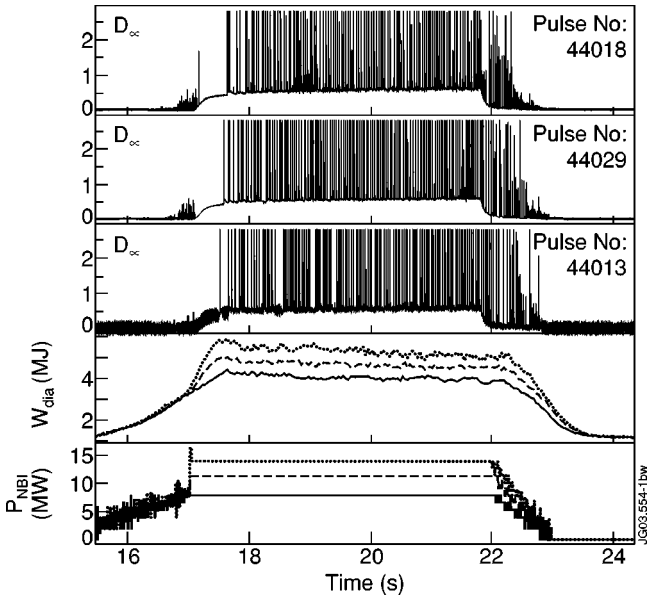

FIG. 1. The time history of the D_α signal measured at the edge of the plasma, the stored energy and the heating power are shown for JET discharges 44018 (8.1 MW, solid line), 44029 (11.3 MW, dashed line), and 44013 (13.9 MW, dotted line). The bottom two panels illustrate the increase of the stored energy with increasing heating power.

time history of the D_α signal measured at the edge of the plasma, as well as the stored energy and the heating power for the three discharges. For each discharge, it can be seen that the stored energy is roughly constant during the quasi-steady state H-mode period from 18.0 s to 20.0 s, and that the stored energy is greater in the discharges with increased heating power.

In Ref. 16, the scaling of the heating power required for the transition from L-mode to H-mode, P_{L-H}, is expressed as

$$P_{L-H}[\mathrm{MW}] = 2.84 A_H^{-1} B_T^{0.82} \bar{n}_{20}^{0.58} R^{1.00} a^{0.81}, \tag{1}$$

where $\bar{n}_{20}$ is the line average density in the unit of 10^{20} particles/m^3. Note, the notation and units used in this paper are described in Table II. Based on Eq. (1), the L–H transition power ranges between 6.4 and 6.6 MW for the three discharges considered. These three JET discharges, 44018, 44029, and 44013, are heated mainly by the NBI heating with the power ranging from 8.1 MW to 13.9 MW, which is significantly higher than the power required for the transition to H-mode.

The temperature, density, and pressure at the top of the pedestal before an ELM crash are given in the last three lines of Table I. Note that the values in Table I are obtained from the ITPA Pedestal Database[17] version 3.1. In this database, the pedestal density and temperatures are found by using a linear fit to each pedestal profile. It can be seen from Table I that the electron pressure and electron temperature at the top of the pedestal increase as the heating power increases, while the electron density at the top of the pedestal remains nearly unchanged. Unfortunately, the value of pedestal width is not available in the database. If one assumes that the pedestal width remains constant as heating power increases, the increasing values of the pedestal parameters, such as pedestal pressure and temperature, are likely to be the result of the improvement in the edge stability. In several experiments, it was found that the pedestal width is independent of the heating power. For example, in Ref. 18, in the Alcator C-MOD experiment where the edge profiles were obtained using high resolution edge Thomson scattering, it was observed that the pedestal width is independent of the heating power.

TABLE II. Notation used in this paper.

Symbol	Units	Description
a	m	Plasma minor radius (half-width)
r	m	Flux surface minor radius (half-width)
R	m	Major radius to geometric Center of each flux surface
ρ		Toroidal flux coordinate
κ		Plasma elongation
δ		Plasma triangularity
B_T	Tesla	Vacuum toroidal magnetic field at R
I_p	MA	Plasma current
A_H	amu	Hydrogenic isotope mass
Z_{eff}		Effective charge
n_l	10^{19} particles/m^3	Line average density
W_{ped}	MJ	Stored energy in pedestal region
$T_{e,\mathrm{ped}}$	keV	Electron temperature at the top of the pedestal
$n_{e,\mathrm{ped}}$	10^{19} particles/m^3	Electron density at the top of the pedestal
$\bar{n}_{20}$	10^{20} particles/m^3	Line average electron density
$p_{e,\mathrm{ped}}$	kPa	Electron pressure at the top of the pedestal
P_{NBI}	MW	NBI heating power

IV. SIMULATION RESULTS AND DISCUSSION

The simulations are carried out during the quasistationary period of the H-mode phase of each discharge (see Fig. 1). Since the experimentally measured edge profiles for these discharges do not have enough resolution to resolve the width of the barrier, the pedestal width is either set equal to 3 cm or is calculated assuming that the width scales with the ion Larmor radius. Other pedestal width scalings that have been proposed include the pedestal width based on magnetic and flow shear stabilization,[19] the pedestal width based on normalized poloidal pressure,[20] or the pedestal width based on ion orbit loss.[21] However, the results presented in this paper regarding the power dependence of the pedestal, do not appear to be sensitive to the scaling used for the pedestal width.

A. JETTO simulations with ELMs triggered by pressure-driven ballooning modes

In this section, simulations are described for the JET power scan discharges, which are carried out using the JETTO code with the assumption that each ELM crash is triggered by a pressure-driven ballooning mode. If anywhere within the pedestal, the normalized pressure gradient, α, exceeds the critical value of the normalized pressure gradient, α_c, that is

$$\alpha \equiv -\frac{2\mu_0 q^2}{\epsilon B_T^2}\frac{\partial p}{\partial \rho} > \alpha_c, \tag{2}$$

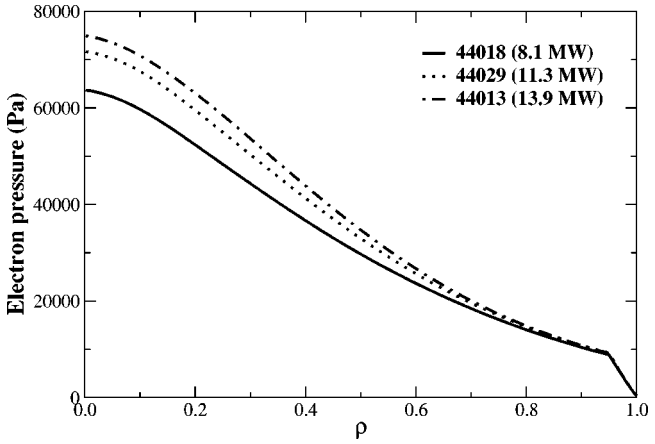

FIG. 2. The predicted pressure profiles are plotted at the time just before ELMs for JET discharges 44018 (8.1 MW), 44029 (11.3 MW), and 44013 (13.9 MW). These simulations are carried out using the JETTO code with ELMs triggered by ballooning mode and a fixed pedestal width of 3 cm.

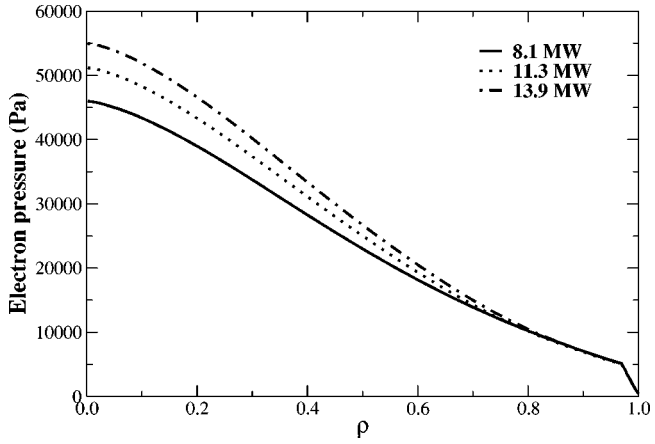

FIG. 3. The predicted pressure profiles are plotted at the time just before ELMs for JET discharges 44018 (8.1 MW), 44029 (11.3 MW), and 44013 (13.9 MW). These simulations are carried out using the JETTO code with ELMs triggered by pressure-driven ballooning mode alone and a pedestal width scales with the Larmor radius.

an ELM crash occurs in the simulation. The numerical value of α_c is chosen and, then, adjusted to be consistent with the HELENA and MISHKA stability code results. The details of the treatment during the crash are described in the Sec. II A.

In Fig. 2, the electron pressure profiles obtained from simulations of discharges 44018, 44029, and 44013 are plotted at the time just before an ELM crash. Note that discharges 44018, 44029, and 44013 have an NBI heating power of 8.1 MW, 11.3 MW, and 13.9 MW, respectively. It can be seen from the figure that the core pressure profiles are higher in the simulation for the discharges with higher heating power, but the pressure at the top of the pedestal is almost same for the three discharges. This result for the pressure at the top of the pedestal is inconsistent with the experimental observation in which the pressure at the top of the pedestal increases with heating power.

The pressure at the top of the pedestal can be approximated by the product of the pedestal width and the pedestal gradient. Consequently, the disagreement between the simulations in Fig. 2 and experimental data could result from the width model. (A fixed value of 3 cm for the pedestal width is used in the simulations shown in Fig. 2.) Therefore, simulations were carried out using a different width scaling in order to test the sensitivity of the simulations to the pedestal width model. Specifically, simulations were carried out for the JET discharges using a pedestal width that scales as the ion Larmor radius. As can be seen in Fig. 3, it is found that the electron pressure at the top of the pedestal is again nearly independent of heating power. Thus, the model in which the pedestal width is a function of the ion Larmor radius combined with ELMs triggered by pressure-driven ballooning modes does not yield simulations that agree with the experimental result of increased pedestal pressure with increased heating power.

B. JETTO simulations with ELMs triggered by current-driven peeling modes

In this section, JETTO simulations for discharges in the JET power scan are carried out with the assumption that each ELM crash can be triggered by current-driven peeling modes. For the ELMs triggered by a current-driven peeling mode, the criterion used is that the current density in the pedestal exceeds a critical current density (which related to the pressure gradient). This critical current density model is based on an analytical expression developed in Ref. 13. For axisymmetric toroidal geometry, the current-driven peeling instability condition is

$$\sqrt{1-4D_M}+C<1+\frac{2}{2\pi q'}\oint\frac{j_{\|}B_T}{R^2B_p^3}dl, \tag{3}$$

where D_M is the Mercier coefficient, which is proportional to pressure gradient; C is a parameter related to the vacuum energy, which is taken to be 0.2 in this study; q' is the derivative of the safety factor with respect to the poloidal flux surface coordinate; $j_{\|}$ is the current density parallel to the magnetic field **B**; R is the major radius; B_p is the poloidal magnetic field; and dl is the poloidal arc length element on a flux surface.

Figure 4 shows the electron pressure profiles obtained from simulations at a time just before an ELM crash for the three discharges 44018 (8.1 MW), 44029 (11.3 MW), and 44013 (13.9 MW). Note that the horizontal scale in Fig. 4 represents only the outer 10% of the plasma. These simulations are carried out with a fixed pedestal width of 3 cm. It can be seen that the values of electron pressure at the top of the pedestal for discharge 44018, 44029, and 44013 are 6.10, 6.52, and 7.33 kPa, respectively, so that the electron pressure at the top of the pedestal increases with the heating power. These results indicate a trend that is similar to the experimental data presented in Table I. From the experimental data, the relation between the electron pressure at the top of the pedestal and the heating power is approximately

$$p_{\mathrm{e,ped,exp}}\propto P_{\mathrm{heating}}^{0.5}. \tag{4}$$

For the simulations using ELMs triggered by current-driven

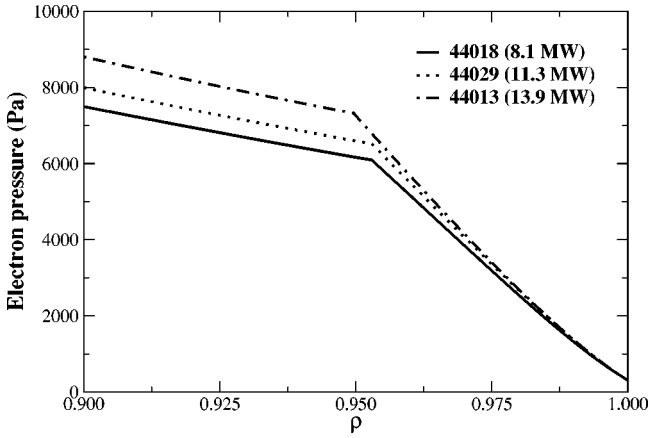

FIG. 4. The predicted pressure profiles are plotted at the time just before ELMs for JET discharges 44018 (8.1 MW), 44029 (11.3 MW), and 44013 (13.9 MW). These simulations are carried out using the JETTO code with ELMs triggered by current-driven peeling modes and a fixed pedestal width of 3 cm.

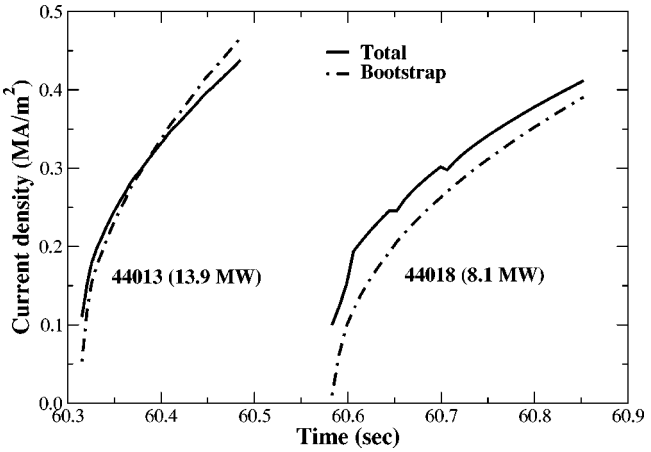

FIG. 6. The plasma current and bootstrap current at a normalized minor radius of 0.97 is plotted as a function of time for the low power (44018) and high power (44013) discharges. These results are obtained from the simulations with ELMs triggered by current-driven peeling modes.

peeling modes, shown in Fig. 4, it is found that the electron pressure at the top of the pedestal scales with the heating power as

$$p_{\mathrm{e,ped,sim}} \propto P_{\mathrm{heating}}^{0.3}. \tag{5}$$

Thus, the simulations with ELMs triggered by current-driven peeling modes yield a somewhat weaker dependence of the electron pressure at the top of the pedestal as a function of heating power than that indicated by experimental data.

Figure 5 shows the simulated plasma current density and bootstrap current density profiles at a time just before an ELM crash for all three discharges. It can be seen in the top panel in Fig. 5 that the current density rises in the steep gradient region of the pedestal at the edge of the plasma and the peak values of the current density in the pedestal region are almost the same for the three discharges. The main contribution to the edge current density is the bootstrap current density shown in the bottom panel in Fig. 5. The bootstrap current density is generated near the edge of the plasma mainly due to the strong pressure gradient within the pedestal. Note that, according to neoclassical theory, the bootstrap

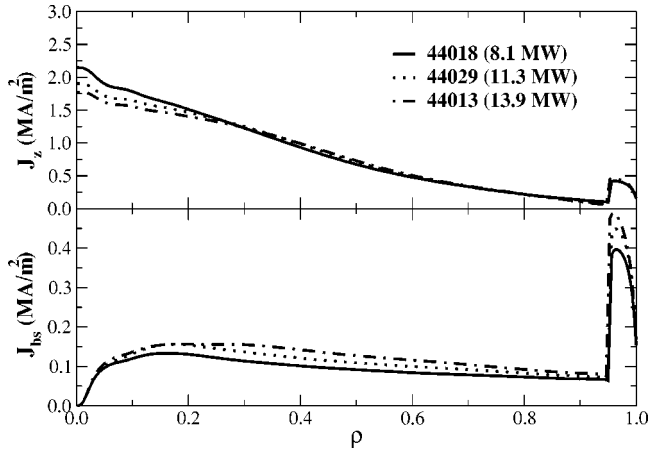

FIG. 5. The plasma current (top panel) and bootstrap current (bottom panel) profiles is plotted at the time just before ELMs for all three discharges.

current density is approximately proportional to the pressure gradient and inversely related to the collisionality.

In Fig. 6, the total current and bootstrap current densities are plotted for the time interval between two consecutive ELM crashes at the normalized minor radius of 0.97 ($r/a = 0.97$) for the low power discharge 44018 and the high power discharge 44013. Note, the normalized minor radius of 0.97 is in the region within the pedestal, close to the top of the pedestal. It can be seen that both the total and the bootstrap current densities rise more quickly after an ELM crash in the higher power discharge than do the corresponding current densities in the low power discharge. At the time just before an ELM crash (at the current peak), it can be seen that the bootstrap current density is lower than the total current density in the low power discharge (44018) while the bootstrap current density exceeds the total current density in the high power discharge (44013). This result can be explained as follows: In the high power discharge (44013), the bootstrap current density increases very quickly due to a rapid rise of pressure gradient, but the rise in the total current density is slowed down by a back electromotive force. As a result, the bootstrap current density is larger than the total current density just before an ELM crash in the higher power discharge. In the low power discharge (44018), the bootstrap current increases more slowly, resulting in a smaller back electromotive force and, as a consequence, the total current density is larger than the bootstrap current density in that case. The simulations indicate that, although the critical current density that results in the current-driven instability is nearly independent of the injected power, the bootstrap current density and the related pressure gradient in the pedestal do increase with increasing power.

C. Stability analysis

Stability analyses are performed to evaluate the edge stability at the time just before an ELM crash for simulations in Fig. 4 using the HELENA and MISHKA MHD stability codes. Note that the simulations in Fig. 4 are carried out with the assumption that each ELM crash is triggered by current-

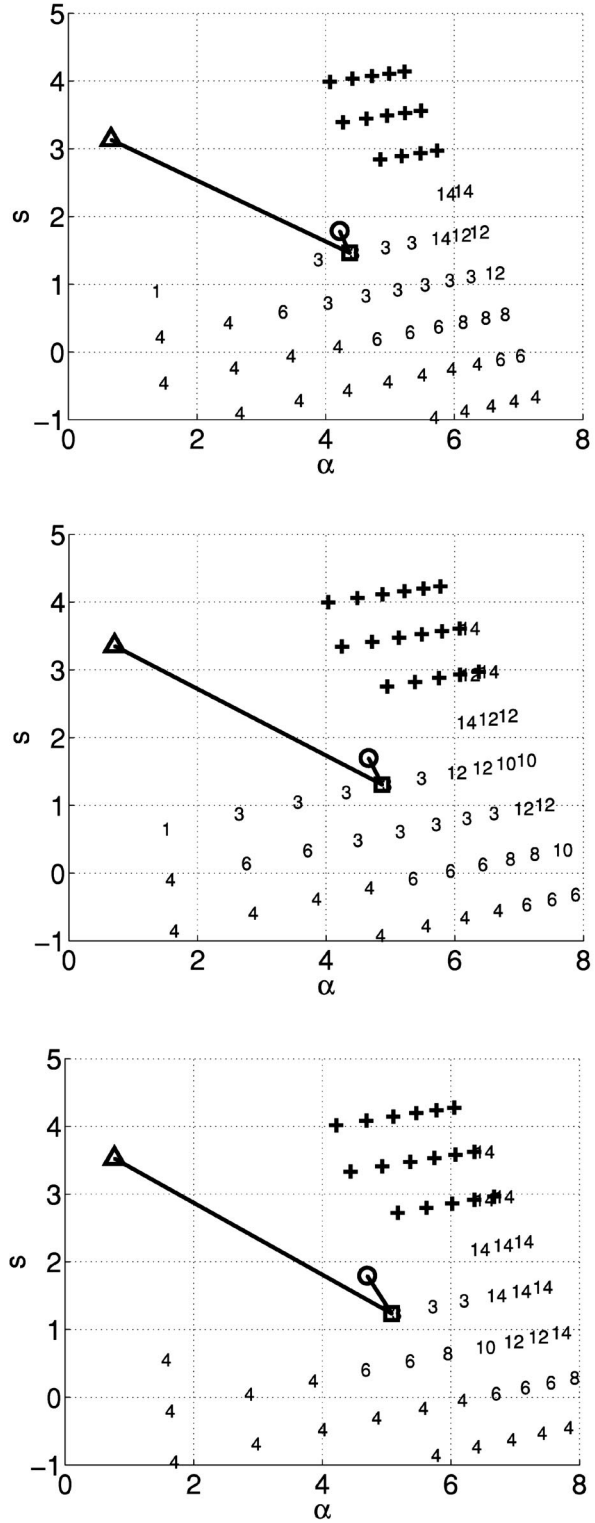

FIG. 7. Stability results obtained using the HELENA and MISHKA stability codes are plotted on an $s-\alpha$ stability diagram for JET discharges 44018 (top panel), 44029 (middle panel), and 44013 (bottom panel). The region of instability associated with the infinite-n ideal ballooning modes is indicated with crosses. The numbers indicate the most unstable finite-n ballooning and low-n kink/peeling modes at each location on the $s-\alpha$ plane. Higher mode numbers ($n \geqslant 10$) correspond to finite-n ballooning modes. The region without numbers or crosses is the region where all modes are stable. The values of s and α at the 92%, 95% (top of the pedestal), and 97% flux surface are indicated by △, □, and ○, respectively.

driven peeling modes. The version of the MISHKA code used in these analyses considers only the ideal MHD modes. On the stability $s-\alpha$ diagrams, the unstable infinite-n ideal ballooning, finite-n ballooning and low-n kink/peeling modes are indicated. The toroidal mode numbers, n, included in the MISHKA code analysis range from 1 to 14.

Figure 7 shows the stability $s-\alpha$ diagrams for discharges 44018 (top panel), 44029 (middle panel), and 44013 (bottom panel). Note that the toroidal mode number n shown on the stability $s-\alpha$ diagram are the most unstable modes. Only unstable modes with the growth rates greater than 0.03 of the Alfvén frequency are included in Fig. 7. A weakly unstable mode might be stabilized if a stabilizing effect such as the finite Larmor radius or the ion diamagnetic drift effect were included. A discussion of this stabilizing effect is beyond the scope of this study. It can be seen that at the 95% flux surface (near the top of the H-mode pedestal), the plasma is unstable to the $n=3$ kink mode in each case. Note that the magnetic shear near the edge of plasma is relatively low for the discharges considered in the power scan. It can also be seen in Fig. 7 that the shape of the unstable regions in the stability $s-\alpha$ diagram are similar, but that the normalized pressure gradient, α, associated with the 95% flux surface increases as the heating power increases. For discharges 44018 (8.1 MW), 44029 (11.3 MW), and 44013 (13.9 MW), the maximum values of the normalized pressure gradient, α, are 4.37, 4.87, and 5.13, respectively.

V. CONCLUSION

Simulations of H-mode discharges in a JET power scan are carried out using the JETTO code. Predictive pedestal and core models are used together in these simulations. It is found that the ELMs triggered by the current-driven peeling modes in these simulations can explain the increase in pedestal pressure as the heating power increases. In the stability analyses carried out for these discharges, it is found that the edge pressure gradient and the edge current density are limited by low-n kink/peeling modes and that the critical pressure gradient increases with plasma heating power.

ACKNOWLEDGMENTS

One author (T.O.) thanks the Royal Thai Government and the Development and Promotion for Science and Technology Talents Project of Thailand (DPST) for their support. This work was conducted partly under European Fusion Development Agreement. It was supported in part by the U.S. Department of Energy (DOE) under Contract No. DE-FG02-92-ER-5414 and by the UK Department of Trade and Industry and by EURATOM.

[1] P. H. Rebut, R. J. Bickerton, and B. E. Keen, Nucl. Fusion **25**, 1011 (1985).
[2] G. Saibene, L. D. Horton, R. Sartori *et al.*, Nucl. Fusion **39**, 1133 (1999).
[3] J. Kinsey, T. Onjun, G. Bateman, A. H. Kritz, A. Pankin, G. M. Staebler, and R. E. Waltz, Nucl. Fusion **43**, 1845 (2003).
[4] T. Onjun, G. Bateman, A. H. Kritz, and G. Hammett, Phys. Plasmas **9**, 5018 (2002).
[5] J. G. Cordey for the ITPA H-mode Database Working Group and the ITPA Pedestal Database Working Group, Nucl. Fusion **43**, 670 (2003).

[6]M. Erba, A. Cherubini, V. V. Parail, and A. Taroni, Plasma Phys. Controlled Fusion **39**, 261 (1997).
[7]A. B. Mikhailovskii, G. T. A. Huysmans, S. E. Sharapov, and W. Kerner, Plasma Phys. Rep. **23**, 844 (1997).
[8]W. A. Houlberg, K. C. Shaing, S. P. Hirshman, and M. C. Zarnstorff, Phys. Plasmas **4**, 3230 (1997).
[9]H. R. Wilson, J. W. Connor, A. R. Field, S. J. Fielding, R. L. Miller, L. L. Lao, J. R. Ferron, and A. D. Turnbull, Phys. Plasmas **6**, 1925 (1999).
[10]P. Gohil, M. A. Mahdavi, L. Lao *et al.*, Phys. Rev. Lett. **61**, 1603 (1988).
[11]G. T. A. Huysmans, T. C. Hender, and B. Alper, Nucl. Fusion **38**, 179 (1998).
[12]G. T. A. Huysmans, T. C. Hender, B. Alper *et al.*, Nucl. Fusion **39**, 1489 (1999).
[13]J. W. Connor, H. R. Hastie, H. R. Wilson, and R. L. Miller, Phys. Plasmas **5**, 2687 (1998).
[14]H. R. Wilson and R. L. Miller, Phys. Plasmas **6**, 873 (1999).
[15]J. Manickam, Phys. Fluids B **4**, 1901 (1992).
[16]R. Aymar, P. Barabaschi, and Y. Shimomura (for the ITER team), Plasma Phys. Controlled Fusion **44**, 519 (2002).
[17]T. Hatae, M. Sugihara, A. E. Hubbard *et al.*, Nucl. Fusion **41**, 285 (2001).
[18]J. W. Hughes, D. A. Mosseessian, A. E. Hubbard, B. LaBombard, and E. S. Marmar, Phys. Plasmas **9**, 3019 (2002).
[19]M. Sugihara, Y. Igitkhanov, G. Janeschitz, A. E. Hubbard, Y. Kamada, J. Lingertat, T. H. Osborne, and W. Suttrop, Nucl. Fusion **40**, 1743 (2000).
[20]T. Osborne, K. H. Burrell, R. J. Groebner, L. L. Lao, A. W. Leonard, R. Maingi, R. L. Miller, G. D. Porter, G. M. Staebler, and A. D. Turnbull, J. Nucl. Mater. **266–269**, 131 (1999).
[21]K. C. Shaing, Phys. Fluids B **4**, 290 (1992).